scientific reports

Check for updates

OPEN

Role of motility and nutrient availability in drying patterns of algal droplets

Anusuya Pal[1,2]✉, Anupam Sengupta[3] & Miho Yanagisawa[4,5,6]

Sessile drying droplets in various bio-related systems attracted attention due to the complex interactions between convective flows, droplet pinning, mechanical stress, wettability, and the emergence of unique patterns. This study focuses on the drying dynamics of *Chlamydomonas reinhardtii* (chlamys), a versatile model algae used in molecular biology and biotechnology. The experimental findings shed light on how motility and nutrient availability influence morphological patterns– a fusion of macroscopic fluid dynamics and microbiology. This paper further discusses the interplay of two competing stressors during drying– nutrient scarcity (quantitative analysis) and mechanical stress (qualitative analysis), where the global mechanical stress does not induce cracks. Interestingly, motile chlamys form clusters under nutrient scarcity due to metabolic stress, indicating the onset of flocculation, a common feature observed in microbial systems. Moreover, non-motile chlamys exhibit an "anomalous coffee-ring effect" in the presence of nutrients, with an inward movement observed near the droplet edge despite sufficient water in the droplet. The quantitative image processing techniques provide fundamental insights into these behaviors in classifying the patterns into four categories (motile+with nutrients, motile+without nutrients, non-motile+with nutrients, and non-motile+without nutrients) across five distinct drying stages– Droplet Deposition, Capillary Flow, Dynamic Droplet Phase, Aggregation Phase, and Dried Morphology.

Keywords Drying droplet, Chlamydomonas, Motility, Nutrient availability, Patterns

Microbial active matter[1] encompasses diverse species, including bacteria, algae, fungi, bacteriophages, and viruses, which are ubiquitous in nature. These systems have been extensively studied at the single-cell level[2], and population levels[3], serving as subjects of fundamental research and various biotechnological applications. Their unique intrinsic traits, such as size, shape, structure, growth characteristics, and responses to external stimuli like temperature, humidity, stress, pH, and nutrient availability[4], have contributed to their scientific significance.

The ongoing research on single-cell biology (primarily in the nano to microscales) has been propelled by innovative tools like micro-arrays, facilitating investigations into cellular behavior at solid-liquid interfaces. Techniques like microfluidics[5] and evaporative drying of droplets[3,6,7] have been used to explore microorganism dynamics on a population level. The evaporative drying process of biologically relevant systems induces convective flow, resulting in collective behavior, self-assembly, mechanical instabilities, and the emergence of macroscopic patterns[4].

Drying of sessile *active droplets*– droplet confining active inclusions like bacteria[6,8,9], bacteriophages[10], spermatozoa[11], nematodes[12], and so on–has recently received considerable attention[13]. The drying droplets containing active biological particles are notably more intricate than passive particles due to the added complexities of motility and micro-environmental influences on fluid flows and self-aggregation. Intriguingly, the "coffee-ring" effect[14] in the active matter-like systems can be altered by bio-surfactants produced by bacteria[7], and various factors, including substrate properties, bacterial strains[15,16], particle characteristics (size, shape), and drying rates[17] impact the resulting deposited patterns. However, it is not limited to only active systems but also includes passive systems such as DNA and nucleic acids[18], polymers[19–22], globular proteins[23], liquid crystal[24,25], blood[26,27], etc. Regardless of the nature of the biologically relevant systems (active or passive), the

[1]Department of Physics, University of Warwick, CV47AL Coventry, UK. [2]Graduate School of Arts and Sciences, The University of Tokyo, Komaba 4-6-1, 153-8505 Meguro, Tokyo, Japan. [3]Physics of Living Matter Group, Department of Physics and Materials Science, University of Luxembourg, Esch-sur-Alzette L-1511, Luxembourg. [4]Komaba Institute for Science, Graduate School of Arts and Sciences, The University of Tokyo, Komaba 3-8-1, 153-8902 Meguro, Tokyo, Japan. [5]Graduate School of Science, The University of Tokyo, Hongo 7-3-1, 113-0033 Bunkyo, Tokyo, Japan. [6]Center for Complex Systems Biology, Universal Biology Institute, The University of Tokyo, Komaba 3-8-1, 153-8902 Meguro, Tokyo, Japan. ✉email: apal@g.ecc.u-tokyo.ac.jp

drying patterns can be influenced by the presence of surfactants, salts, nanoparticles, etc., in the droplet and the type of solvent (water to organic solvents).

In recent years, an exciting avenue has emerged in disease diagnosis in sessile drying droplet studies. The distinctive patterns that emerge during the drying process not only have the potential to differentiate various diseases but can also offer valuable insights into the disease's developmental stage[4]. Furthermore, previous models of droplet drying include many studies[22,28–30]. However, these models are based on a number of simplifying assumptions about the drying droplet. To the best of our knowledge, no models have yet examined active matter systems, which could provide insights into the roles of motility and nutrient availability.

Recent advancements in biomaterials and tissue engineering have underscored the remarkable potential of *Chlamydomonas reinhardtii* (henceforth chlamys) as a versatile candidate for various applications. It spans from growth factor delivery in wound healing scaffolds to an oxygen source in respiratory failure or organ transplantation scenarios[31]. Chlamys exhibits tailored responses depending upon stressors such as oxygen levels, light intensity, nutrient availability, and toxins, demonstrating remarkable adaptability to even hostile micro-environments[32]. Its optimal size, mechanosensitivity, and capacity for biocompatible cell wall modification without releasing toxins upon decomposition further enhance its appeal, rendering it a superior choice for drug delivery compared to other flagellated microbes[33]. Notably, these chlamys elucidate the molecular underpinnings of specific human ciliary diseases, including ciliary dyskinesia and ailments linked to cystic kidneys[34]. This newfound focus on chlamys has revealed insights into the intricate mechanisms underlying these diseases, shedding light on potential therapeutic avenues.

Despite being extensively studied at the population level (generally in the micro to macro scales), investigating chlamys in sessile drying droplet settings remains limited. Though recent advancements in the study of evaporating active matter-like droplets focusing on hydrodynamics are reviewed in[35,36], only one study has explored chlamys drying droplets, analyzing the impact of light stimuli on its responses and resultant patterns– linked to motility[3]. However, nutrient conditions beyond motility, a crucial determinant, remain unexplored. Across diverse species, nutrient availability is known to impact motility and vice-versa[37], yet the coupling between motility, physiology, and pattern formation in drying algal droplets remains an unexplored entity. This paper presents experimental findings of the drying process and pattern formation of chlamys droplets by quantifying the images and incorporating statistical modeling to address this research gap. In this context, the drying process functions as an engine, propelling the droplet (system) from one equilibrium state to another. The study aims to address

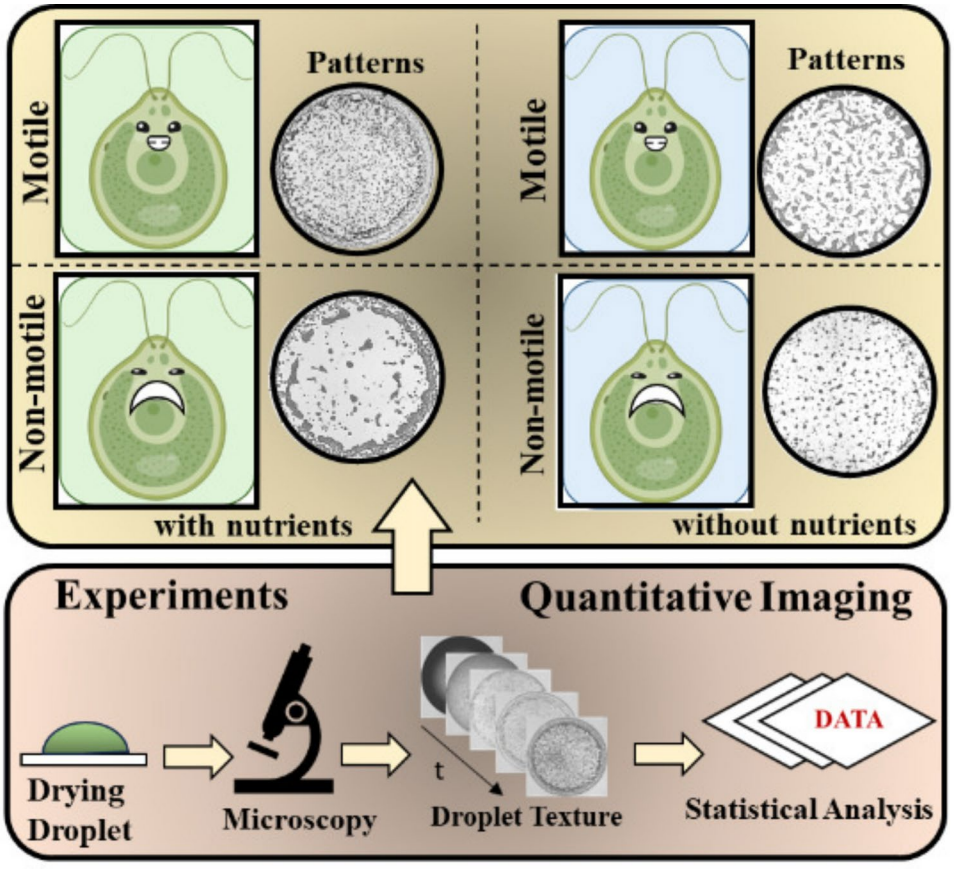

Fig. 1. It explores the drying behavior of four distinct *Chlamydomonas reinhardtii* algal droplets (motile+with nutrients, motile+without nutrients, non-motile+with nutrients, and non-motile+without nutrients). It unfolds the motility-nutrient effects on the morphological patterns by using simple drying droplet experiments with the help of quantitative image analysis and textural statistical analysis.

four primary inquiries: (i) What role does the motility of chlamys play in shaping pattern dynamics during the drying process? (ii) Does motility and nutrient availability correlate in determining drying patterns, and if so, how do they interact? (iii) What are the distinct drying stages, and which stage is most influential in shaping these patterns? (iv) How do textural responses evolve throughout the drying stages, including mean, standard deviation, skewness, and kurtosis? Do these responses facilitate the classification of emerging patterns into four classes: motile+with nutrients, motile+without nutrients, non-motile+with nutrients, and non-motile+without nutrients? Figure 1 illustrates the methodology employed in this study, aimed at advancing our fundamental understanding of chlamys droplet drying behavior by exploiting image quantification and statistical analysis.

Results and discussions

Visual interpretation of the drying evolution in chlamys droplets

Figure 2(I-IV) presents the evolving drying progression of both motile and non-motile chlamys droplets, with and without nutrient availability. The contact angle and the height of these droplets exhibit a consistent monotonic decrease [see Figure S1 of the supplementary section], aligning with behavior observed in other bio-colloids[23,38]. However, it is to be noted that the density of non-motile chlamys typically falls within the range of approximately $1.0 - 1.2\ gcm^{-3}$, which closely matches that of the external medium, in this case, water. This similarity in density results in a relatively low sinking velocity for chlamys, as there is minimal density mismatch with the surrounding fluid. Consequently, this low sinking velocity is unlikely to cause the chlamys to precipitate or froth within the droplet during evaporation. This behavior contrasts with passive bio-colloids, which are very small-sized particles, leading to different dynamics.

Over time, the texture of the images transitions from dark to light, as showcased in Figure 2(I-IV). Notably, all chlamys droplets undergo four distinct stages, completing the drying process within 300-350 seconds. In Stage 1, the droplet deposition (DD) stage, the droplet adopts a spherical cap shape upon being placed onto the coverslip (substrate). The evaporative flux is highest in the vicinity of the three-phase contact line. Notably, the droplet size in this study (with a diameter of $\sim$2 mm) remains below the capillary length threshold. Consequently, surface tension prevails over gravity, preventing the droplet from flattening onto the substrate. All droplets are found

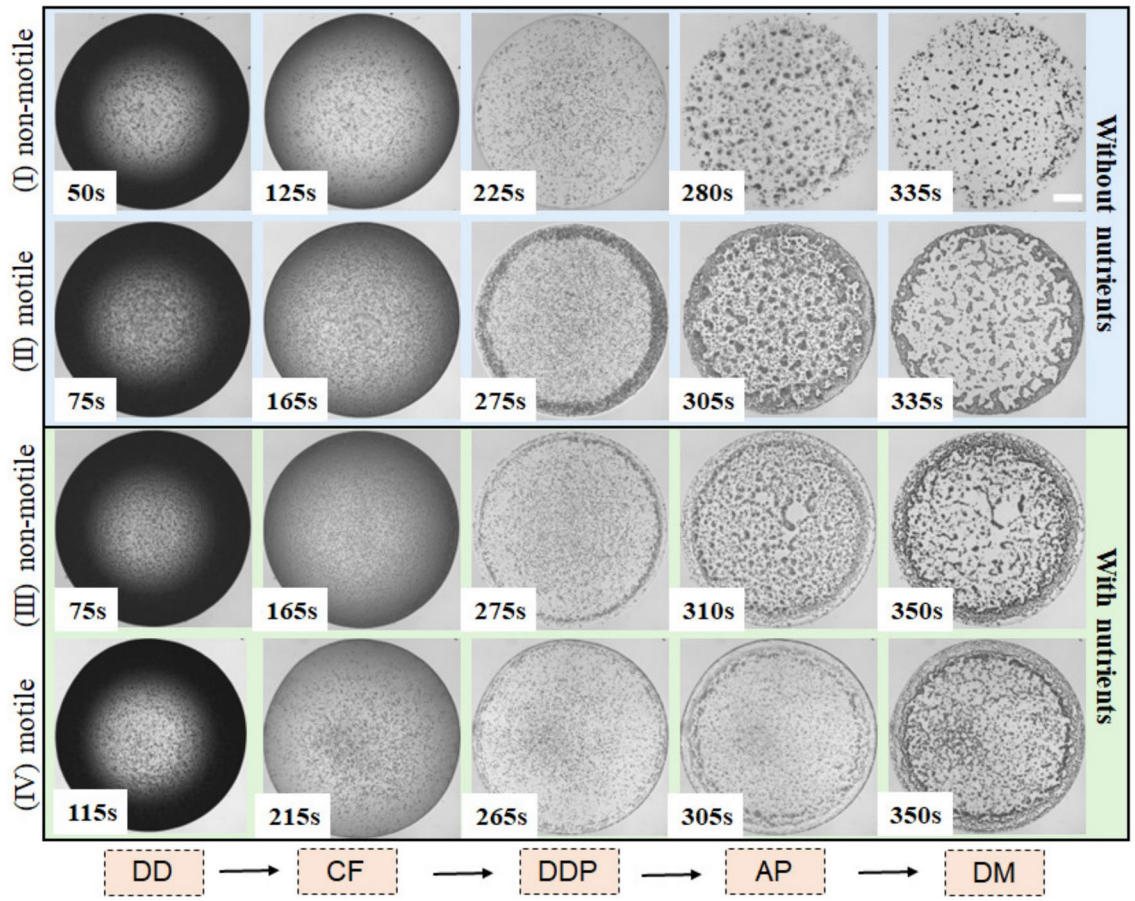

Fig. 2. Drying evolution of chlamys droplets of various classes: (**I**) without nutrients+non-motile, (**II**) without nutrients+motile, (**III**) with nutrients+non-motile, and (**IV**) with nutrients+motile. The arrows show the time (t) evolution of the dynamic patterns during drying. Different drying stages include Droplet Deposition (DD), Capillary Flow (CF), Dynamic Droplet Phase (DDP), Aggregation Phase (AP), and Dried Morphology (DM). The scale bar of length 0.3 mm is shown with the white rectangle in the top-right panel.

to be pinned throughout the drying process. The control experiments were performed only with the fluids, excluding the chlamys, to address this persistent pinning across classes (motile vs. non-motile with and without nutrients). The pinning of these droplets emerges in the presence of the nutrients, i.e., the droplets containing the broth (containing salts, proteins, and potentially surface-active components), implying that residual TAP medium particles contribute to droplet pinning [see Figure S2(I) of the supplementary section]. In contrast, the drying evolution does not show any pinning and residual deposit for the droplets containing pure de-ionized water (without nutrients) [see Figure S2(II) of the supplementary section].

The contrast of dark black near the periphery and gray within the central region arises due to the droplet's curvature, as depicted in Figure 2(I-IV) DD stage. While internal convective flow ensues during this period, the subsequent stage (Stage 2) is marked by dominant outward capillary flow (CF), promoting the movement of chlamys toward the droplet's edge. To better understand what happens in this CF stage, measuring the flow fields with and without chlamys and in the presence or absence of the nutrients is crucial. However, it is beyond the scope of our current study. Furthermore, the visuals show that most chlamys concentrate near the droplet's periphery, generating the well-known "coffee-ring" effect[14]. However, this phenomenon is less pronounced in non-motile chlamys droplets lacking nutrients. These could be attributed to different factors. For example, the interaction of the chlamys with the bottom surface and the liquid-air interface in this sessile drying droplet configuration could be different based on the motility and the fluid with or without nutrients. Thus, the "coffee-ring" effect may be enhanced or inhibited depending on the specific interactions between the chlamys and the interfaces. These interface interactions are beyond the scope of our current study and are intended to be in our future investigations.

This drying stage, termed the Dynamic Droplet Phase (DDP), is particularly distinctive for all droplet types– motile and non-motile, with and without nutrient availability. As the drying process advances, water evaporation leads to chlamys aggregation (Figure 2(I-IV) AP– aggregation phase), a process characteristically short, requiring 10-25 seconds. In this stage, however, we see that the fluid front proceeds from the periphery to the central region, promoting the self-assembly and aggregation of chlamys in a chaotic way. The DDP and AP stages, being highly dynamic and unique, ultimately dictate the final patterns within the Dried Morphology (DM) stage (see Figure 2(I-IV) Stage DM). Therefore, merely analyzing the dried patterns without considering the underlying dynamics would only provide a superficial understanding. By investigating the dynamics of the droplets as they dry, we can uncover the mechanisms and interactions that drive the formation of these patterns. These mechanisms are examined in the following sections (Section 2.2-2.4).

Chlamys droplets in the presence of nutrients

Figure 3(I-II)a-f provides a step-by-step illustration of the evolving drying dynamics for both motile and non-motile chlamys in the presence of nutrients. A visual representation of the underlying physical mechanism driving this pattern formation is depicted in Figure 3(III).

For the case of motile chlamys [Figure 3(I)a-f], smaller-sized chlamys (with sizes of $3-5\ \mu$m) tend to accumulate at the droplet's periphery. Interestingly, larger-sized chlamys (with sizes of $7-9\ \mu$m) do not gather at the contact line. The relatively larger size of these chlamys prevents them from reaching the extreme edge of the droplet. As time progresses, the chlamys gather near the droplet's periphery, forming a distinct "coffee-ring" pattern[14]. As observed in previous studies, this size-dependent phenomenon could lead to segregation[39].

Interestingly, once most chlamys are transported towards the periphery [Figure 3(I-II)c-d and yellow arrows in Figure 3(IV-V)], an inward movement of chlamys becomes evident in the presence of a sufficient amount of water. The unusual point observed here is the movement directionality of the chlamys. They initially move towards the edge of the droplet in the presence of sufficient water, and after a while, they take an inward direction yet predominantly stay near the droplet's edge. A continuation of this inward movement to the central region of the droplet could have been attributed to a weak capillary flow and dominant Marangoni flow. However, in this instance, this is not the case. This anomalous behavior is not limited to this specific active system; similar patterns have been reported in other drying passive systems[40]. However, the unique aspect is this inward movement's dependence on the chlamys' motility. For the motile case, the smaller-sized transported chlamys become trapped at the very edge of the droplets while only the larger-sized counterparts move inward. Figure S3 of the supplementary section depicts the histogram of different-sized chlamys. A geometric model that supports this inward motion is formulated using the relationship $\tan\theta = r/L$, where θ represents the contact angle of the droplet, r denotes the radius of the chlamys, and L signifies the distance the chlamys move inward. With chlamys radius $r \sim 4.5\ \mu m$ and inward movement distance $L \sim 25\ \mu m$ (quantified using ImageJ[41]), the calculated θ is 10.2°. This aligns closely with the experimentally observed $\theta = 12-10^{\circ}$ obtained from contact angle measurements (shown in Figure S1 of the supplementary section).

In contrast, the non-motile chlamys do not show such phenomena. All the chlamys move inward, and a homogeneous texture appears at the very edge of the droplet [Figure 3(I-II)e-f and Figure 3(III)c-d]. This characteristic behavior implies that the motility of the chlamys plays a significant role in dictating these patterns. The two most important questions include: (a) What mechanisms propel chlamys' inward migration toward the droplet's center while largely remaining at the droplet's edge (described as the "anomalous coffee-ring" effect)? and (b) What accounts for the discrepancy in the inward movement between motile and non-motile chlamys?

The inward migration of chlamys in the drying droplets likely results from a complex interplay of several factors, viz., (i) Hydrodynamic trapping: in the motile case, smaller-sized chlamys are likely to be trapped at the droplet's edge due to hydrodynamic effects. As the droplet evaporates, fluid flow patterns generated by the motile cells could create regions of stagnation or recirculation near the edge, where smaller cells are retained. Conversely, the larger cells may have sufficient momentum to overcome these trapping effects and move inward. (ii) Size-dependent interactions: the differential behavior of smaller and larger-sized chlamys could be due to size-dependent interactions with the droplet-substrate interface. Smaller cells will likely experience stronger

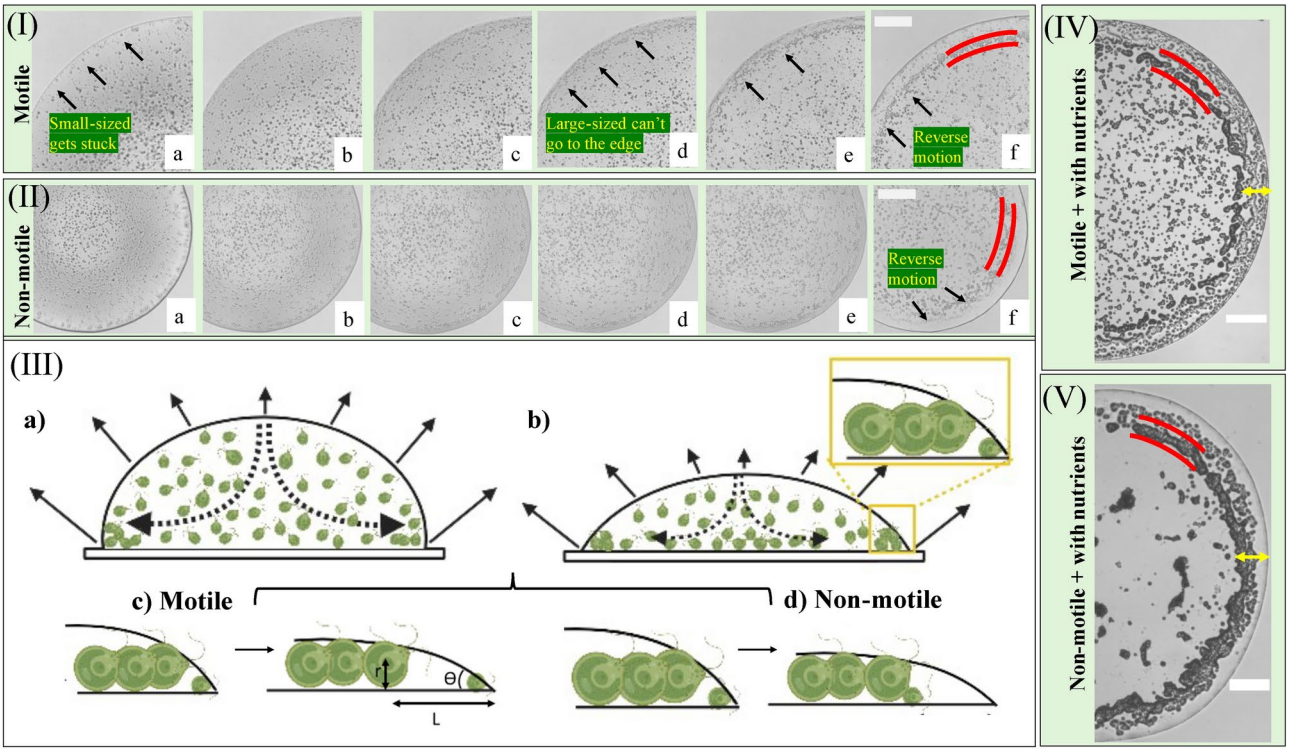

Fig. 3. (**a**-**f**) Time evolution of the (**I**) motile and (**II**) non-motile chlamys in the nutrient-rich environment. The images are captured under $10\times$ magnification. (**III**) A physical mechanism in which (**a**-**b**) Stages DD and CF in the droplet are displayed. Stages DDP is shown in **c** and **d**, with motile and non-motile chlamys, respectively. The θ represents the contact angle of the droplet, r denotes the radius of the chlamys, and L signifies the distance the chlamys move inward. The unique patterns in DM Stage for the (**IV**) motile and (**V**) non-motile chlamys are exhibited, where the red lines depict the deposited chlamys near the periphery, and the yellow arrows dictate the "coffee-ring" width. A scale bar has a length of 0.2 mm.

adhesion forces or surface tension effects that anchor them near the edge. In comparison, larger cells are less affected and can migrate inward more freely. Moreover, the size of chlamys (3-9 μm) is larger than that of typical bacterial systems (0.2-2 μm)[9]. This larger size may explain why the bacteria (at least those examined in the context of drying droplets) do not exhibit the same anomalous behavior, even though both chlamys and bacteria are considered active matter systems. (iii) Cell-cell interactions: in the motile case, the interactions between chlamys may also play a role. Larger cells will create a barrier or shield effect, preventing smaller cells from moving past them and being trapped at the edge. This behavior could contribute to cell size segregation within the droplet. Additionally, the accumulation of small-sized chlamys might enhance pinning at the three-phase contact line; the secretion of polymer-like substances[7] from these chlamys, especially under mechanical[42]or metabolic stress, is also possible.

However, decoupling the inward motion of chlamys (motile or non-motile) from the background hydrodynamic field and understanding the exact mechanisms for answering the above two questions would require further investigation. This could involve examining the hydrodynamic field alone, analyzing the behavior of chlamys separately for both motile and non-motile cases, or exploring the interaction of chlamys with the generated hydrodynamic fields. Such an investigation would be experimentally complex and is beyond the scope of the current study.

Notably, the droplets under consideration do not show any buckling or cracking as the drying process progresses. As the drying process nears completion, the chlamys aggregate due to the decreasing fluid content, resulting in the formation of relatively larger accumulated structures. This aggregation phenomenon is universal in sessile bio-colloidal drying droplets, irrespective of whether the particles are passive[43] or active[7]. The rapid evaporation of trapped water between neighboring aggregates leads to their displacement to some extent [red lines in Figure 3(I-II)f and (IV-V)]. The AP stage captures the aggregation of the chlamys due to significant water loss, and the final morphological patterns are observed in the DM stage as the drying concludes. Notably, both non-motile and motile chlamys droplets exhibit a ring width of $0.17 - 22$ mm (quantified using Image]^{41}), indicated by the yellow arrow in Figure 3(IV-V)]. This stage provides a distinctive fingerprint-like pattern visually [Figure 3(IV-V)], highlighting the differences between patterns arising from motile and non-motile chlamys droplets in the presence of nutrients.

The videos of the motile and non-motile chlamys in the presence of nutrients during the drying process in the bright-field configurations are provided in the supplementary section as SV1 and SV2, respectively.

Quantitative analysis of chlamys droplets in the presence of nutrients

The preceding section demonstrated an inward motion of the chlamys. However, the specific nature of this motion remained unclear. A quantitative image analysis in the DDP stage for motile and non-motile droplets in the presence of nutrients is conducted to address this. All the images are converted into binary images using ImageJ[41] in this stage. These processed time-sequenced images in the form of video for motile and non-motile chlamys are provided in the supplementary section [see SV3 and SV4]. The time intervals are divided into four stages, viz., initial, middle_1, middle_2, and final [see Figure 4(I-IV)]. The motile and non-motile cases are shown in Figure 4(I-IV), where (II) and (IV) depict representative images, respectively. The green line and the arrow in Figure 4(I and III) display the movement of chlamys for the region of interest (A to B), as shown with a rectangular box (outlined in black color) in Figure 4(II and IV). The averaged gray values are plotted as a function of the radial distance. The x-axis is the radial distance (in μm), where the starting point (zero) corresponds to the end of the droplet edge [i.e., the pinned edge, shown with a black dotted line in Figure 4(I-IV)].

The quantification of chlamys movement is approximately 25 μm over 100 seconds for the motile case, whereas it is approximately 50 μm over 7 seconds for the non-motile case [Figure 4(I-IV)]. The inward velocity for the motile and non-motile chlamys is calculated to be ~ 0.4 μm s^{-1} and ~ 7 μm s^{-1}, respectively. A high value of non-motile case suggests that the microbial cells were carried away by an external flow of similar magnitude. The small motile cells obstructing the flow trigger a lower effective speed in the larger motile cells. This phenomenon is widely observed in microbial systems where cells are known to swim against the flow in closed paths, the so-called *Jeffrey orbits*[44]. The faster inward transportation of the non-motile chlamys compared to their motile

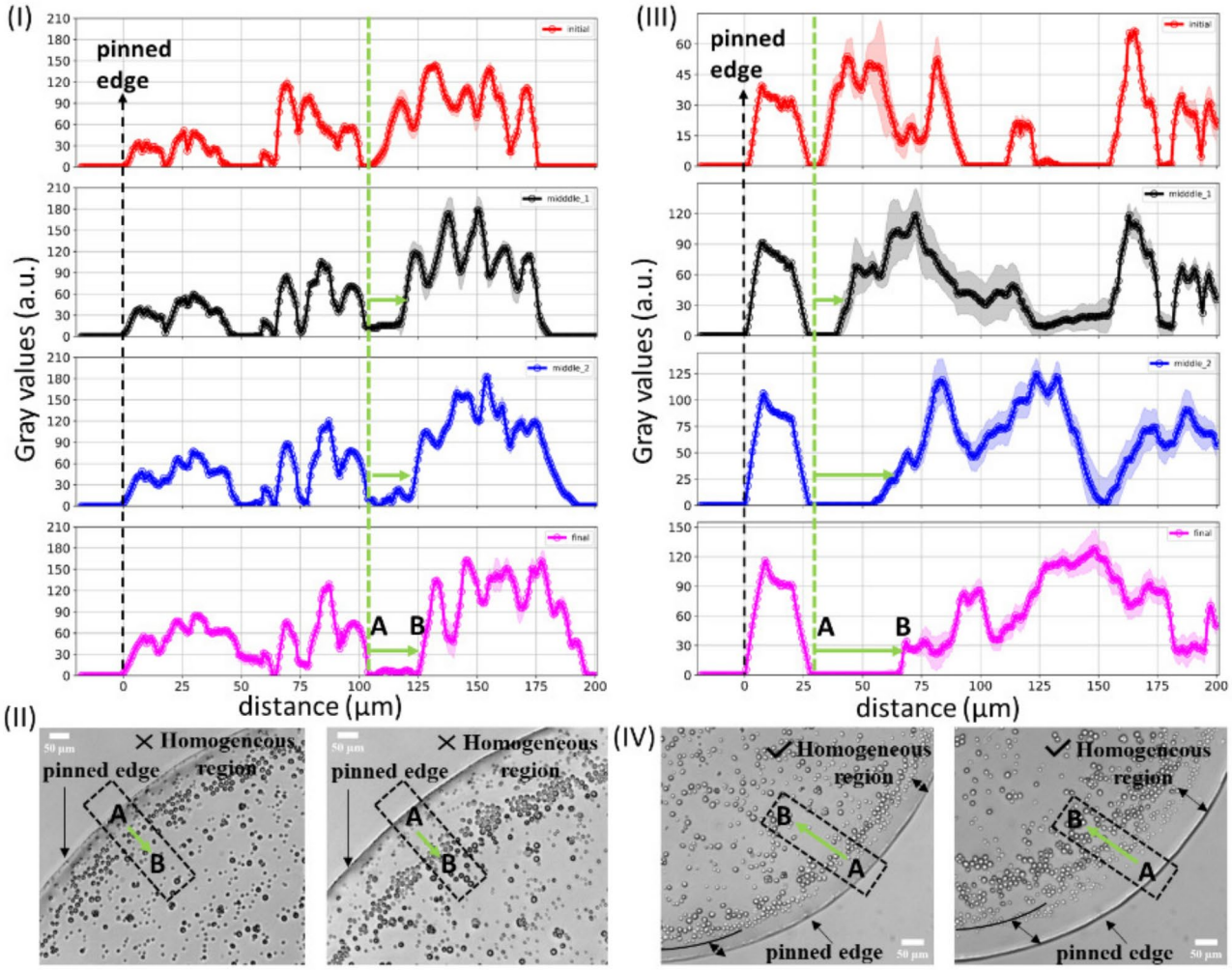

Fig. 4. (**I-IV**) Quantitative image analysis of chlamys dynamics in the DDP drying stage: time-sequenced images of motile and non-motile droplets are processed into binary, and the time is divided into four stages, viz., initial, middle_1, middle_2, and final sub-stages. (**I**) and (**III**) depict the averaged gray values (a.u.) against radial distance (x-axis in μm) from the end of the droplet edge (i.e., the pinned edge, displayed in black dotted lines) for the motile and non-motile cases, with (II) and (IV) showing the region of interest (outlined in black) considered in this analysis. The green lines and arrows in (**I**) and (**III**) illustrate their movement from regions A to B. The shaded error shows the standard deviation of the measurements of the gray values aggregated during these sub-stages.

counterparts may initially seem counterintuitive. Several factors are likely to contribute to this phenomenon: (i) Uniform inward movement: the non-motile chlamys cannot swim actively or respond to environmental cues. As a result, they may uniformly move inward without needing to navigate or overcome obstacles, leading to a more efficient and rapid inward transport than motile cells. (ii) Reduced resistance: the motile chlamys actively propel themselves through the fluid, encountering resistance from both the fluid and interactions with other cells. In contrast, the non-motile cells experience less resistance and faster transportation as they are carried passively by fluid flow within the droplet. (iii) Collective behavior: in the motile case, the trapped smaller chlamys at the droplet edge and the inward movement of larger chlamys lead to a heterogeneous distribution and slower overall transport. In contrast, the non-motile populations that lack this variability in cell size may exhibit more uniform and efficient inward movement, leading to homogeneous texture near the edge.

Interestingly, this heterogeneity is also reflected in Figure 4(I and III), where the line profiles of the binary images during the middle and final sub-stages of DDP exhibit non-zero values for the motile case. In contrast, the gray value intensity remains consistently zero for the non-motile case throughout their inward movement. It confirms the position of the trapped motile chlamys (displayed in white in the binary images) along the way for the motile case. However, all the chlamys are transported inward for the non-motile case, resulting in a homogeneous texture. These distinct behaviors lead to the unique patterns drawn in Figure 3(IV-V). The response function bridges macroscopic fluid dynamics and microscopic microbial behavior, facilitating a fusion of macroscopic pattern dynamics and microbiology.

Chlamys droplets in the absence of nutrients

The drying progression and pattern formation of motile and non-motile chlamys in the absence of nutrients are depicted in Figure 5(I-VII). In Figure 5(I)a-c, most chlamys move towards the droplet's periphery via capillary flow. The inward motion of these transported chlamys is similarly observed (Figure 5(I)d-f), albeit a weaker movement compared to the movement of the chlamys when the nutrients are present. The formation of diverse clusters in the presence of ample water inside the droplet marks the emergence of a fascinating noble phenomenon of the motile chlamys without nutrients in the DDP stage. In the meantime, the neighboring chlamys converge, creating small clusters that subsequently merge into larger ones. As time elapses (Figure 5(I)g-l), these clusters also exhibit rotational motion. The calculated cluster counts are highlighted with red labeled boxes in the zoomed image (Figure 5(I)j). Smaller clusters housing 5-7 chlamys each are marked in blue (Figure 5(II)). A histogram in Figure 5(III) illustrates the distribution of chlamys numbers per cluster, varying from ~ 13 to ~ 59, averaging around 34. The presence of individual cluster instances is shown in Figure S4 of the supplementary section. The videos of the motile and non-motile chlamys in the absence of nutrients during the drying process in the bright-field configurations are provided in the supplementary section as SV5and SV6 respectively.

The cluster formation is represented in Figure 5(IV). The chlamys initiate interacting and assembling into clusters with the progression of drying progress. The cluster formation phenomenon is similar to other systems reported in earlier studies[45]. However, it's crucial to note that our chlamys droplets are most likely driven by the dynamic Marangoni flows, intricate concentration gradients, and metabolic stress, leading to complex dynamics in pattern formation. The cluster formation initially resembles chains of 3-4 chlamys, followed by ordered arrangements of 6-10 chlamys, and these clusters merge to form larger entities. While this ordered configuration isn't sustained longer, cluster formation remains consistent until the significant water evaporates in the AP stage. SV7and SV8in the supplementary section depict motile chlamys drying without the nutrients. SV7illustrates chlamys dynamics under sufficient water availability, while SV8shows cluster formation.

Exploring the hidden mechanism behind the observed characteristics reported in this paper is crucial. The sealed chamber experiments confirm this cluster formation (Figure S5 in the supplementary section) and establish that the drying process does not play a role. This cluster formation of chlamys is more likely attributable to metabolic stressed conditions. This behavior indicates the onset of flocculation, a well-known behavior in motile microbial species[46,47]. Flocculation is a strategic survival mechanism for chlamys under starvation conditions, allowing them to aggregate or merge to survive nutrient scarcity[32,48]. Notably, this flocculation phenomenon occurs during the drying stage when an optimal amount of water is still present (in the DDP stage), well before the initiation of the AP stage. The report of flocculation in drying bacterial systems is rare, even under similar starved conditions[9]. This disparity can be attributed to the time scale of flocculation (t_{flocc}) being significantly longer than the drying time (t_{drying}) for bacterial suspensions, given their smaller size range of 1-2 μm. In contrast, chlamys, being approximately five times larger, exhibit a faster flocculation time scale ($t_{\mathrm{flocc}} < t_{\mathrm{drying}}$), allowing them to undergo such aggregative behaviors within the drying droplets. This differential time scale underscores a potentially unique adaptive advantage conferred by the larger size of chlamys, allowing them to exhibit flocculation dynamics within the constrained temporal framework of the drying process.

A similar coffee-ring width of ~ 0.2 mm (quantified using ImageJ[41]) is also observed, irrespective of the availability of the nutrients. However, a consistent trend was missing when the cluster diameter and the number of chlamys in each cluster were plotted as a function of the radial distance (distance measured from the center). Even the cluster diameter normalized by the corresponding "coffee ring width" as a function of the radial distance did not show any consistent trend (see Figures S6-S7 in the supplementary section).

In contrast, non-motile chlamys without nutrients do not exhibit significant coffee-ring patterns (Figure 5(VI-VII)). Figure 5(VI)a-l shows the time evolution of non-motile chlamys. These are uniformly deposited compared to other conditions, a phenomenon different from what is reported in[3]. It's plausible that the differences observed in the patterns of non-motile cells could be attributed to variations in their preparation methods. The existing literature indicates that the composition and history of active-matter samples can significantly influence the resulting patterns[4]. Figure 5(VII) displays the morphological outcome of the post-drying state. Table 1 presents different events occurring during the drying process of chlamys of different classes, i.e., non-motile + with nutrients, motile + with nutrients, non-motile + without nutrients, and motile + without nutrients.

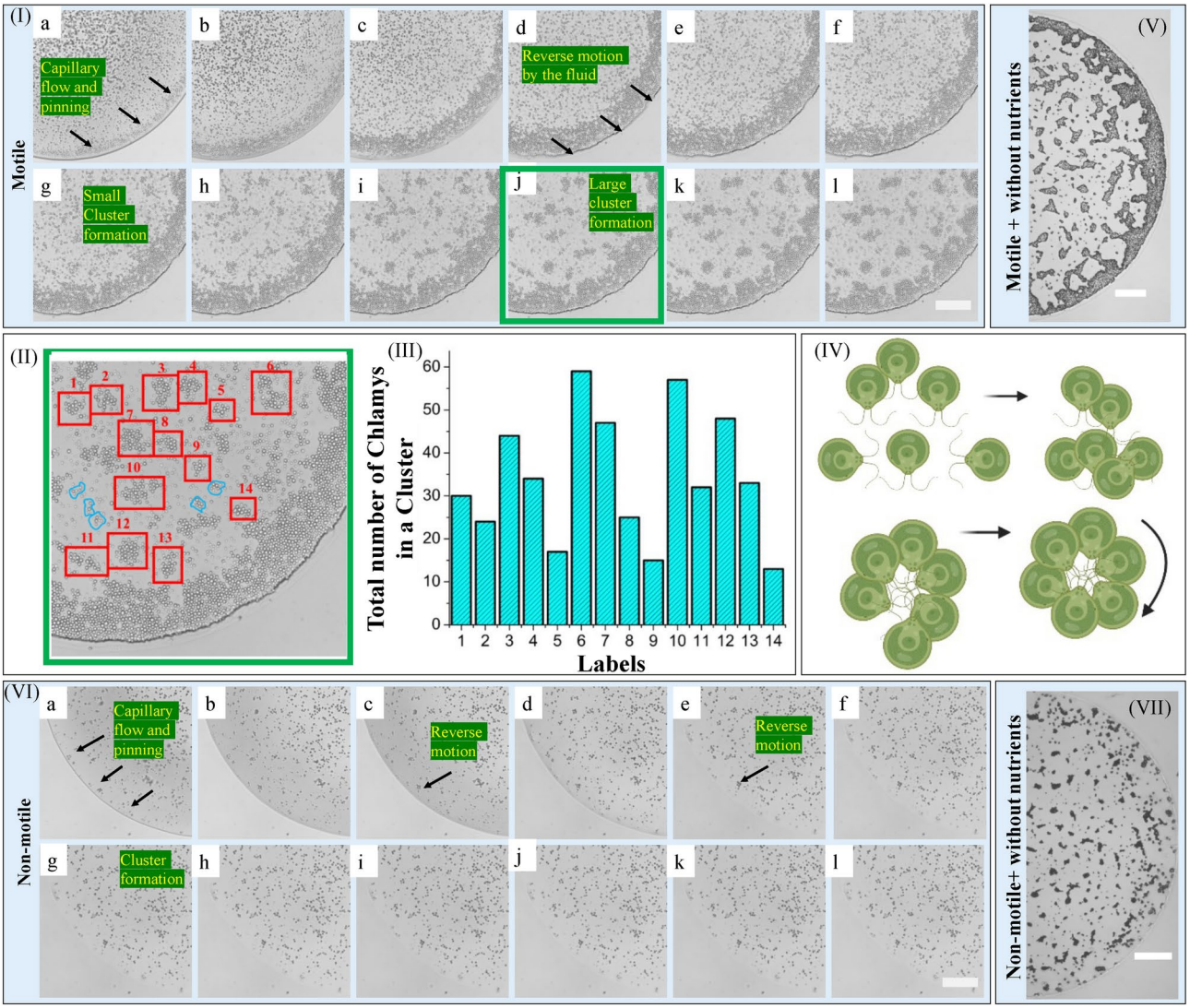

Fig. 5. (**I**)a-l: Time evolution of the motile chlamys in the nutrient-deficient environment. The images are captured under 10× magnification. (**II**) Zoomed view (green) of (**I**)j displaying clusters outlined in red with labels and small clusters in blue. (**III**) A histogram showing the total number of chlamys in each red-labeled cluster. (IV) Cluster formation in the DDP stage due to metabolic stress. (V) Dried morphological patterns of the motile chlamys. (**VI**)a-l Time evolution and (**VII**) Dried morphological patterns of the non-motile chlamys in the nutrient-deficient environment. A scale bar has a length of 0.2 mm.

Stages	Characteristics	Analysis	Motile + without nutrients	Non-motile + without nutrients	Motile + with nutrients	Non-motile + with nutrients
DD	Spherical-cap shape (dark & gray texture)	Qualitative	YES	YES	YES	YES
CF	Different flows	Qualitative	YES (faster move)	YES (slower move)	YES (faster move)	YES (slower move)
DDP	Coffee-ring	Quantitative	YES	NO (uniform deposition)	YES	YES
	Cluster formation	Quantitative	YES	NO	NO	NO
AP	Aggregation	Qualitative	YES	YES	YES	YES
	Crack formation (due to mechanical stress)		NO	NO	NO	NO
DM	Droplet pinning	Quantitative	YES	YES	YES	YES
	Unique patterns		YES	YES	YES	YES
	Anomalous coffee-ring		YES (very weak)	YES (very weak)	YES (weak)	YES (predominant)

Table 1. Summary of different events occurring in the drying droplets of motile and non-motile chlamys with and without nutrients. The different stages include Droplet Deposition (DD), Capillary Flow (CF), Dynamic Droplet Phase (DDP), Aggregation Phase (AP), and Dried Morphology (DM).

Classification of droplets using textural statistics

Figure 6(I-VIII) illustrates the drying evolution of the textural parameters, including mean, standard deviation (SD), skewness (Skew), and kurtosis (Kur) for motile and non-motile chlamys droplets, with and without nutrients. These parameters capture various statistical features within the droplet area.

The mean value initially experiences a slow increase during the droplet deposition (DD) stage, followed by a rapid rise in the capillary flow (CF) stage, with a variation of ~ 15 a.u. and ~ 50 a.u., respectively. Subsequently, a minimal change or fluctuation in the mean value is observed during the dynamic droplet phase (DDP). A dip occurs in the aggregation (AP) stage, leading to a decrease of ~ 15 a.u. The Mean, however, increases to a saturated range in the final dried morphology (DM) stage. The standard deviation (SD) ranges from ~ 15 a.u. to ~ 45 a.u. The general trend is a slow increase in the DD stage, followed by a rapid decrease in the CF stage. However, the DDP stage exhibits distinct characteristics for each type of chlamys droplet. For instance, motile chlamys droplets display a hump-like feature in the presence of nutrients during the DDP stage, while a slow increase is observed in their absence [see Figure 6(III and VII)]. Non-motile chlamys droplets show minimal fluctuations in the presence of nutrients, whereas a slight decrease is observed without nutrients. The AP stage is the shortest phase, characterized by a rapid rise followed by a decrease until the saturation point in the DM stage. Notably, during the DDP stage, the SD captures different details while the mean remains relatively constant. During the AP, the complexity intensifies, resulting in a sharp increase in the SD values [see Figure 6(I, III, V, and VIII)].

The skewness (Skew) exhibits a decreasing trend until the DDP stage, after which it increases during the AP stage. Following this, the values stabilize, similar to the mean and SD values. While the Skew does not display a distinct pattern for motility and nutrient availability, the kurtosis (Kur) exhibits notable trends during the DDP and AP stages. In the DDP stage, the Kur exhibits a linear trend, with an adjusted R^2 value of 0.89-0.96, although the slope values differ. The slope for motile chlamys droplets with and without nutrients is $\sim 0.03 s^{-1}$ and $-0.006 s^{-1}$, respectively. In contrast, the slope values for non-motile chlamys droplets with and without nutrients are $\sim 0.01 s^{-1}$ and $\sim 0.04 s^{-1}$, respectively. In the AP stage, the Kur decreases in the presence of nutrients, regardless of motility. However, in the absence of nutrients, it increases for motile chlamys, while it alternately increases and decreases for non-motile chlamys droplets [see Figure 6(II, IV, VI, and VIII)].

An intriguing observation arises when examining the skewness vs. kurtosis plot (see Figure S8(I-II) in the supplementary section). Skew and Kur offer valuable insights into data distribution and shape. The data is symmetric and balanced when the nutrients are present. Conversely, the non-appearance of such a clear pattern in skewness-kurtosis relationships in the absence of the nutrients suggests a more complex and diverse distribution (see Figure S8(I) in the supplementary section). Notably, from Figure 6, the AP and DM stages exhibit a chaotic appearance, indicating higher variability and unpredictability in chlamys droplet behaviors during these stages. Indeed, the skewness-kurtosis plot can unveil interesting insights into system dynamics. For instance, considering all stages, scattered data points along negatively skewed values suggest greater diversity or complexity in behavior. However, focusing on the first three stages (DD, CF, and DDP) of chlamys drying reveals a specific trend (symmetry) in the plot (Figure S8(II) in the supplementary section). The alignment of data points

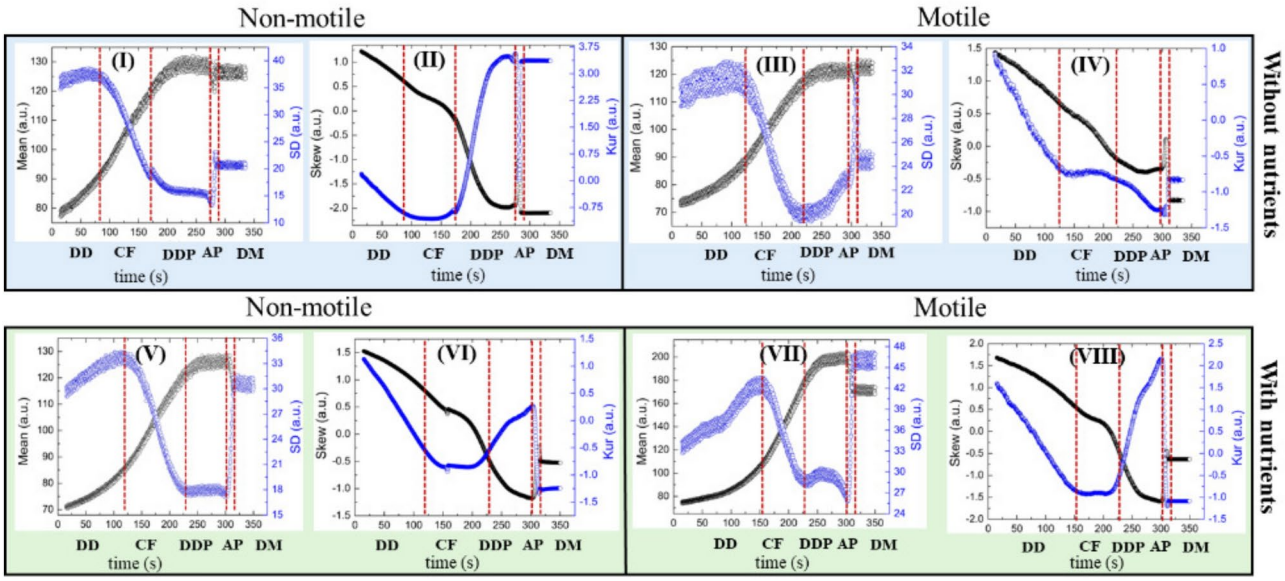

Fig. 6. (**I-VIII**) Drying evolution of the statistical textural image parameters, the Mean, standard deviation (SD), skewness (Skew) and kurtosis (Kur) [in arbitrary units, (a.u.)] of motile and non-motile chlamys droplets with and without nutrients. The black lines depict the Mean and Skew values, whereas the blue lines draw the SD and Kur values. Different stages are highlighted by red lines: Droplet Deposition (DD), Capillary Flow (CF), Dynamic Droplet Phase (DDP), Aggregation Phase (AP), and Dried Morphology (DM). The x-axis represents time (in seconds) during the drying process.

within a specific region indicates consistent behavior or arrangement of chlamys particles during those stages. This symmetry persists until the DDP stage, only to break down with the advancement of the drying process. Understanding subtle changes in statistical parameters like skewness and kurtosis across different drying stages can offer crucial insights into underlying mechanisms and dynamics. Such information could potentially guide the development of refined models or theories, aiding the explanation of observed behaviors and guiding further experimental exploration.The analysis of the textural parameters (Mean, SD, Skew, and Kur) not only helps in quantifying the evolving stages of the drying process in the droplets but also reveals the distinctive behaviors (flow and transport of chlamys, aggregation, and the morphological patterns) between motile and non-motile chlamys in the presence or absence of nutrients. A one-way ANOVA test was performed to examine the possible significant interactions among four classes, viz., (a) motile+with nutrients, (b) motile+without nutrients, (c) non-motile+with nutrients, and (d) non-motile+without nutrients based on textures. The post hoc test is also conducted to examine pairwise differences between groups.

The results confirm significant differences among the four classes across the entire drying process in terms of Mean ($F[3, 5356] = 377.71, p < 0.001$), SD ($F[3, 5356] = 377.71, p < 0.001$), Skew ($F[3, 5356] = 239.8, p < 0.001$), and Kur ($F[3, 5356] = 462.89, p < 0.001$). Similar differences are observed when considering individual stages separately, supporting the hypothesis that the drying process varies across classes. Additionally, the five drying stages are statistically distinguishable, as depicted in the quantitative analysis of Figure 6(I-VIII). The average values of the textural parameters captured for the entire drying process and the DM stage are displayed as bar plots in Figure 7(I-II). In Figure 7(I), mean, SD, and Skew fail to distinguish between motile+without nutrients and non-motile+with nutrients, whereas kurtosis distinguishes all four classes. Skewness also fails to identify differences between with and without nutrients for motile chlamys droplets. This underscores the importance of feature selection in classification tasks. However, distinct patterns, depicted in Figure 2(I-IV), emerge during the progression of the drying process. Pairwise comparisons support this observation, confirming that all textural parameters can statistically distinguish the four combinations for the DM stage [see Figure 7(II)]. For instance, the SD of motile+with nutrients is significantly higher than that of motile+without nutrients, followed by non-motile+with nutrients and non-motile+without nutrients. These distinct trends observed in textural statistics during different drying stages provide a robust basis for training machine learning algorithms that could potentially automate the classification process and offer deeper insights into the complex behavior of chlamys droplets under varying conditions.

The limitation of this study is that it does not provide a clear mechanism for the non-motile chlamys, which exhibit a dominant 'anomalous coffee-ring effect' in the presence of nutrients, characterized by inward movement near the droplet edge despite sufficient water content. This could be investigated using standard optical techniques, including fluorescence and confocal microscopy, or by applying microparticle image velocimetry to high-speed imaging with high frame rates. However, such investigations are beyond the scope of this current study and are intended for future work.

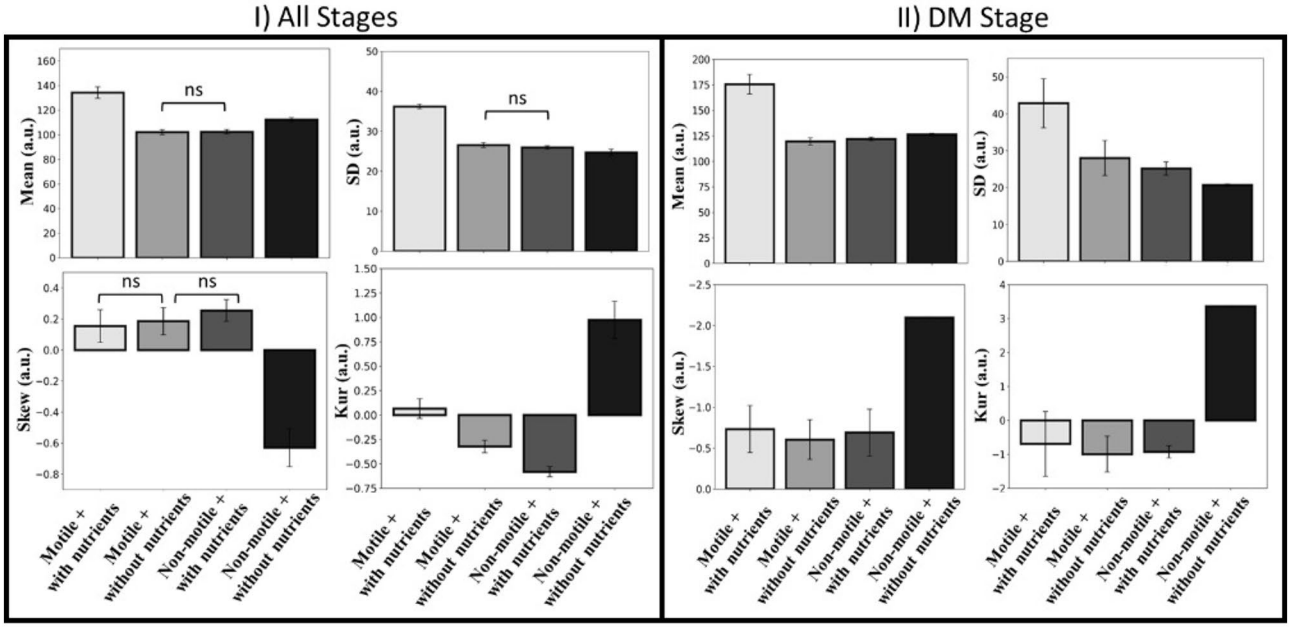

Figure 7. The pair-wise comparison of the non-motile and motile chlamys with and without nutrients for different textural image statistical parameters: Mean, Standard deviation (SD), Skewness (Skew), and Kurtosis (Kur). Statistical significance is indicated by $p < 0.05$, with "ns" representing non-significant pairs. This analysis is conducted for two stages of the drying process: (**I**) the entire drying process considering all stages and (**II**) the Droplet Morphology (DM). The error bars correspond to the standard deviation of each aggregated textural measurement.

In conclusion, this study draws the multifaceted potential of *Chlamydomonas reinhardtii* (chlamys) as an exceptional algal model in the context of sessile drying droplets cross-linking the micro and macro length scales. Different image analyses on chlamys have unraveled the interplay between motility-nutrient interactions, nutrient scarcity, and mechanical stress during drying. The five distinct drying stages, viz., Droplet Deposition (DD), Capillary Flow (CF), Dynamic Droplet Phase (DDP), Aggregation Phase (AP), and Dried Morphology (DM), provide a comprehensive understanding of the intricate processes underlying drying dynamics. Notably, mechanical stress is ineffective in inducing cracks. On the other hand, nutrient deficiency induces stress in chlamys, fostering aggregation, unity, and cluster formation in the motile chlamys when ample water is present in the droplet. The "anomalous coffee-ring effect" predominantly observed in the non-motile chlamys in the presence of nutrients provides new insights into the correlation between nutrient availability and motility. The quantitative image analysis and statistical significance confirm that the patterns in the DM stage can be identified into four different classes (motile+with nutrients, motile+without nutrients, non-motile+with nutrients, and non-motile+without nutrients). The droplet drying can be used as a simple classification tool, opening promising avenues for the bio-behavioral responses to external stimuli. Notably, the insights gained from this study hold applicability beyond chlamys, extending to various microorganisms, contributing to the understanding of the drying process, and catalyzing advancements in the interdisciplinary research domains spanning microbiology, fluid dynamics, and active matter physics.

Methods

Cell culture, samples, and the preparation procedures

Chlamys, a eukaryotic microorganism, boasts dimensions of ~ 10 μm in length and possesses flagella measuring around 10 μm[49]. Notably, the algal strain CC-124 features an eyespot– an organelle sensitive to light– enabling phototaxis. Although a flagellum's primary role involves propelling cellular motion, it also serves as a sensory apparatus, responding to chemical, mechanical, and environmental cues such as temperature and humidity. Intriguingly, CC-124 demonstrates negative phototaxis, signifying a tendency to move away from light sources.

The chlamys strain CC124 cultures were cultivated axenically using a Tris-Acetate-Phosphate (TAP) medium[50] at 21°C under continuous fluorescent illumination (100 μ E m^{-2} s^{-1}, OSRAM Fluora). The light-dark cycle followed a 12-hour cycle each. The TAP medium composition comprises Tris base, TAP Salts Stock Solution, Hutner's Trace Metal Solution, Glacial or anhydrous acetic acid, and phosphates, which facilitate cell synchronization. During the exponential growth, harvesting was done at $7 - 10 \times 10^6$ cells mL^{-1}, and daily transfers were made to a fresh phosphate-buffered medium. The growth rate was monitored daily; only healthy cells were used in this experiment. The growth curve is illustrated in Figure S9(I), and cell motility is depicted in S9(II) of the supplementary section. Two conditions were examined: (i) optimal nutrient availability and (ii) without nutrients, i.e., de-ionized water (DI). For the experiment with DI, sub-sampled cells were centrifugated at ~ 800 r.p.m. for ~ 10 minutes[51]. The supernatant was then exchanged with deionized water (DI) from Millipore, with a resistance of 18.2MΩ.cm. To induce cell immobility, ~ 1 μL of Iodine solution, acting as a red dye, was introduced to the eppendorf tubes containing 1.5 mL of the algal solution. This mixture was left undisturbed for roughly ~ 10 minutes. Experiments involving motile cells were executed seconds after sample preparation, mitigating the possibility of any cell lysis (if present) before the drying phase.

~ 1 μL of each prepared sample was pipetted onto a microscopic coverslip (Catalog number 48366-045, VWR, USA), forming a circular droplet with a radius of ~ 1 *mm*. All experiments were conducted under ambient conditions, encompassing a room temperature of $\sim 25^{\circ}$C and a relative humidity of ~ 50 %. Each experiment was replicated twice to ensure reproducibility. The morphological dried patterns of each chlamys are illustrated in Figure S10 of the supplementary section.

Image acquisition

The progression of droplet drying was captured at a rate of 4 frames per second (fps) utilizing a FLIR camera (Catalog no KCC-REM-PGR-GS41) mounted on a Nikon Eclipse E200 microscope, employing bright-field illumination. To prevent any phototactic response from the cells, a long-pass filter with a cut-off wavelength of 765 nm was integrated into the optical pathway. Time recording was initiated upon droplet deposition onto the coverslip. Images were captured at a resolution of 1600×1600 pixels. The lamp intensity remained constant throughout the drying process to maintain minimal fluctuations in background (coverslip) intensity. Before image processing, a calibration slide converted pixel values to real-space lengths. All images were transformed into 8-bit grayscale for enhanced clarity.

The temporal evolution of the contact angle of the chlamys solution during drying was assessed using the drop shape analyzer (DSA 100, KR$\ddot{U}$SS, GmbH). The normalized contact angle and the height of the droplet apex to drying time are depicted in Figure S1 of the supplementary section. The normalization is drawn with respect to the initial contact angle.

Image processing

All time-sequenced images in the DDP stage were converted into binary using ImageJ[41] to quantify the inward movement of the motile and non-motile chlamys and analyze the characteristics of these drying droplets. The binary images feature a black background, with the chlamys appearing in white. A specific rectangular region of interest (ROI) is selected for a length of 332 pixels and a height of 73 pixels. The same ROI is kept for both non-motile and motile cases. The *line profile* tool is used, and the gray values as a function of the radial distance (in μm) for each image are extracted as a .CSV file. The radial distance's starting point (zero) is shifted so that it corresponds to the droplet edge. To facilitate the analysis, we divided the DDP stage into distinct sub-stages-initial, middle_1, middle_2, and final. We merged all the .CSV files for these sub-stages, and the gray values are averaged. The shaded error shows the standard deviation of these gray value measurements during the sub-

stages. Finally, the plot between the gray values and radial distance provides a distribution of chlamys within the droplet and how these move inward over time for both non-motile and motile cases.

We also employed the *oval tool* within ImageJ[41] to define a circular region of interest (ROI) on the image. Notably, the 8-bit image encompasses gray values spanning from 0 to 255. Our assessment revolved around four essential textural first-order statistics (FOS), namely, the Mean, standard deviation (SD), kurtosis (Kur), and skewness (Skew). These FOS parameters were then extracted from the 8-bit gray images. Subsequently, these textural parameters were harnessed as a feature vector.

Statistical analysis

After identifying the distinct drying stages– Droplet Deposition (DD), Capillary Flow (CF), Dynamic Droplet Phase (DDP), Aggregation Phase (AP), and Dried Morphology (DM), we want to examine possible significant interactions among four classes. For this, a parametric one-way ANOVA test was performed, where the feature vector [Mean, Standard Deviation (SD), Kurtosis (Kur), and Skewness (Skew)] were the dependent variables. The class is the independent factor, with four levels (groups): motile+with nutrients, motile+without nutrients, non-motile+with nutrients, and non-motile+without nutrients. Ideally, a repeated measures ANOVA would have been performed to analyze the data, considering the multiple measurements taken over time. However, the data for each stage (time duration) was unbalanced, potentially affecting the validity of the repeated measures analysis due to class imbalance. To mitigate this issue and ensure robustness, we opted to conduct a one-way ANOVA instead. This approach allowed us to assess the differences in means across different groups while accounting for the unbalanced nature of the data, providing reliable insights into the effects of the independent variable on the dependent variable. The significant level is kept as $p < 0.05$. A pairwise comparison between all the classes is calculated using the Bonferroni test in R (Version 3.6.3) embedded with R studio (Version 1.2.1335, RStudio, Inc., Boston, MA, USA). The *library(rstatix)* and the function *anova_test()* are used for the ANOVA test. The post hoc analysis is performed using Tukey's HSD test using the function *tukey_hsd()*, identifying which groups are significantly different based on the dependent variable.

Data availability

The data that support the findings of this study are available with the corresponding author and may be made available upon reasonable request.

Received: 13 December 2023; Accepted: 20 September 2024
Published online: 08 October 2024

References

1. Sengupta, A. Microbial active matter: A topological framework. *Frontiers in Physics***8** (2020).
2. Drescher, K., Goldstein, R. E., Michel, N., Polin, M. & Tuval, I. Direct measurement of the flow field around swimming microorganisms. *Physical Review Letters***105**, 168101 (2010).
3. Bittermann, M. R., Bonn, D., Woutersen, S. & Deblais, A. Light-switchable deposits from evaporating drops containing motile microalgae. *Soft Matter***17**, 6536–6541 (2021).
4. Pal, A., Gope, A. & Sengupta, A. Drying of bio-colloidal sessile droplets: Advances, applications, and perspectives. *Advances in Colloid and Interface Science***314**, 102870 (2023).
5. Juang, Y.-J. & Chang, J.-S. Applications of microfluidics in microalgae biotechnology: A review. *Biotechnology journal***11**, 327–335 (2016).
6. Thokchom, A. K., Swaminathan, R. & Singh, A. Fluid flow and particle dynamics inside an evaporating droplet containing live bacteria displaying chemotaxis. *Langmuir***30**, 12144–12153 (2014).
7. Sempels, W., Dier, R. D., Mizuno, H., Hofkens, J. & Vermant, J. Auto-production of biosurfactants reverses the coffee ring effect in a bacterial system. *Nature Communications***4** (2013).
8. Kang, Y. K. *et al.* Simple visualized readout of suppressed coffee ring patterns for rapid and isothermal genetic testing of antibacterial resistance. *Biosensors and Bioelectronics***168**, 112566 (2020).
9. Majee, S. *et al.* Spatiotemporal evaporating droplet dynamics on fomites enhances long term bacterial pathogenesis. *Communications Biology***4** (2021).
10. Huang, Q., Wang, W. & Vikesland, P. J. Implications of the coffee-ring effect on virus infectivity. *Langmuir***37**, 11260–11268 (2021).
11. Ríos-Ramírez, M., Reyes-Figueroa, A., Ruiz-Suárez, J. & González-Gutiérrez, J. Pattern formation of stains from dried drops to identify spermatozoa motility. *Colloids and Surfaces B: Biointerfaces***169**, 486–493 (2018).
12. Peshkov, A., McGaffigan, S. & Quillen, A. C. Synchronized oscillations in swarms of nematode turbatrix aceti. *Soft Matter***18**, 1174–1182 (2022).
13. Araújo, N. A. *et al.* Steering self-organisation through confinement. *Soft Matter***19**, 1695–1704 (2023).
14. Deegan, R. D. *et al.* Capillary flow as the cause of ring stains from dried liquid drops. *Nature***389**, 827 (1997).
15. Susarrey-Arce, A. *et al.* Pattern formation by staphylococcus epidermidis via droplet evaporation on micropillars arrays at a surface. *Langmuir***32**, 7159–7169 (2016).
16. Susarrey-Arce, A. *et al.* Bacterial footprints in elastic pillared microstructures. *ACS Applied Bio Materials***1**, 1294–1300 (2018).
17. Richard, E., Dubois, T., Allion-Maurer, A., Jha, P. K. & Faille, C. Hydrophobicity of abiotic surfaces governs droplets deposition and evaporation patterns. *Food Microbiology***91** (2020).
18. Ye, Y., Hao, Y., Ye, M., Song, X. & Deng, Z. Evaporative drying: A general and readily scalable route to spherical nucleic acids with quantitative, fully tunable, and record-high dna loading. *Small***18**, 2202458 (2022).
19. Fujisawa, S., Daicho, K., Yurtsever, A., Fukuma, T. & Saito, T. Molecular dynamics of drying-induced structural transformations in a single nanocellulose. *Small* 2302276 (2023).
20. Liu, Y. *et al.* Three-dimensional coffee-ring effect induced deposition on foam surface for enhanced photothermal conversion. *Small* 2207822 (2023).
21. Bhardwaj, R., Fang, X., Somasundaran, P. & Attinger, D. Self-assembly of colloidal particles from evaporating droplets: role of dlvo interactions and proposition of a phase diagram. *Langmuir***26**, 7833–7842 (2010).
22. Wang, Z., Orejon, D., Takata, Y. & Sefiane, K. Wetting and evaporation of multicomponent droplets. *Physics Reports***960**, 1–37 (2022).
23. Pal, A., Gope, A., Athair, A. S. & Iannacchione, G. S. A comparative study of the drying evolution and dried morphology of two globular proteins in de-ionized water solutions. *RSC Advances***10**, 16906–16916 (2020).

24. Pal, A., Gope, A. & Iannacchione, G. S. A comparative study of the phase separation of a nematic liquid crystal in the self-assembling drying protein drops. *MRS Advances***4**, 1309–1314 (2019).
25. Pal, A., Gope, A. & Iannacchione, G. S. Hierarchical exploration of drying patterns formed in drops containing lysozyme, pbs, and liquid crystals. *Processes***10**, 955 (2022).
26. Pal, A., Gope, A., Obayemi, J. D. & Iannacchione, G. S. Concentration-driven phase transition and self-assembly in drying droplets of diluting whole blood. *Scientific reports***10**, 1–12 (2020).
27. Pal, A., Gope, A. & Iannacchione, G. Temperature and concentration dependence of human whole blood and protein drying droplets. *Biomolecules***11**, 231 (2021).
28. Lohse, D. & Zhang, X. Physicochemical hydrodynamics of droplets out of equilibrium. *Nature Reviews Physics***2**, 426–443 (2020).
29. A new model for a drying droplet. *International Journal of Heat and Mass Transfer***122**, 451–458 (2018).
30. Sazhin, S. S. *et al.* A simplified model for bi-component droplet heating and evaporation. *International Journal of heat and mass transfer***53**, 4495–4505 (2010).
31. Schenck, T. L. *et al.* Photosynthetic biomaterials: a pathway towards autotrophic tissue engineering. *Acta biomaterialia***15**, 39–47 (2015).
32. de Carpentier, F., Lemaire, S. D. & Danon, A. When unity is strength: the strategies used by chlamydomonas to survive environmental stresses. *Cells***8**, 1307 (2019).
33. Arrieta Payares, L. M., Gutiérrez Púa, L. D. C., Di Mare Pareja, L. A., Paredes Méndez, S. C. & Paredes Méndez, V. N. Microalgae applications to bone repairing processes: A review. *ACS Biomaterials Science & Engineering***9**, 2991–3009 (2023).
34. Wijffels, R. H., Kruse, O. & Hellingwerf, K. J. Potential of industrial biotechnology with cyanobacteria and eukaryotic microalgae. *Current opinion in biotechnology***24**, 405–413 (2013).
35. Gelderblom, H., Diddens, C. & Marin, A. Evaporation-driven liquid flow in sessile droplets. *Soft matter* (2022).
36. Wilson, S. K. & D'Ambrosio, H.-M. Evaporation of sessile droplets. *Annual Review of Fluid Mechanics***55**, 481–509 (2023).
37. Sengupta, A. *et al.* Active reconfiguration of cytoplasmic lipid droplets governs migration of nutrient-limited phytoplankton. *Science Advances***8**, eabn6005 (2022).
38. Pal, A., Gope, A., Kafle, R. & Iannacchione, G. S. Phase separation of a nematic liquid crystal in the self-assembly of lysozyme in a drying aqueous solution drop. *MRS Communications***9**, 150–158 (2019).
39. Liu, W., Midya, J., Kappl, M., Butt, H.-J. & Nikoubashman, A. Segregation in drying binary colloidal droplets. *ACS nano***13**, 4972–4979 (2019).
40. Weon, B. M. & Je, J. H. Capillary force repels coffee-ring effect. *Physical Review E***82**, 015305 (2010).
41. Abràmoff, M. D., Magalhães, P. J. & Ram, S. J. Image processing with imagej. *Biophotonics International***11**, 36–42 (2004).
42. Devadasu, E. & Subramanyam, R. Enhanced lipid production in chlamydomonas reinhardtii caused by severe iron deficiency. *Frontiers in Plant Science***12**, 615577 (2021).
43. Yu, Y.-S., Wang, M.-C. & Huang, X. Evaporative deposition of polystyrene microparticles on pdms surface. *Scientific reports***7**, 14118 (2017).
44. Ishimoto, K. Jeffery's orbits and microswimmers in flows: A theoretical review. *Journal of the Physical Society of Japan***92**, 062001 (2023).
45. Hokmabad, B. V., Nishide, A., Ramesh, P., Krüger, C. & Maass, C. C. Spontaneously rotating clusters of active droplets. *Soft matter***18**, 2731–2741 (2022).
46. Roccuzzo, S. *et al.* Metabolic insights into infochemicals induced colony formation and flocculation in scenedesmus subspicatus unraveled by quantitative proteomics. *Frontiers in Microbiology* 792 (2020).
47. Kiørboe, T. & Hansen, J. L. Phytoplankton aggregate formation: observations of patterns and mechanisms of cell sticking and the significance of exopolymeric material. *Journal of Plankton Research***15**, 993–1018 (1993).
48. Gerde, J. A., Yao, L., Lio, J., Wen, Z. & Wang, T. Microalgae flocculation: impact of flocculant type, algae species and cell concentration. *Algal research***3**, 30–35 (2014).
49. Jeanneret, R., Contino, M. & Polin, M. A brief introduction to the model microswimmer chlamydomonas reinhardtii. *The European Physical Journal Special Topics***225**, 2141–2156 (2016).
50. Goldschmidt-Clermont, M., Malnoe, P. & Rochaix, J.-D. Preparation of chlamydomonas chloroplasts for the in vitro import of polypeptide precursors. *Plant Physiology***89**, 15–18 (1989).
51. Jeanneret, R., Pushkin, D. O., Kantsler, V. & Polin, M. Entrainment dominates the interaction of microalgae with micron-sized objects. *Nature communications***7**, 12518 (2016).

Acknowledgements

This research is supported by the Department of Physics at the University of Warwick, UK, and the Graduate School of Arts and Sciences at The University of Tokyo, Japan. A. Pal would like to thank M. Polin, Associate Professor at the University of Warwick, for his valuable support, and the Leverhulme Trust (Grant No. RPG-2018-345). A. Pal and M. Yanagisawa also extend their gratitude to the Japan Society for Promotion of Science (JSPS), KAKENHI Grant No. 23KF0104, for supporting this work. A. Pal expresses appreciation for the JSPS International Postdoctoral Fellowship for Research in Japan (Standard) for the period 2023-25. M. Yanagisawa thanks JST FOREST Program (Grant no. JPMJFR213Y) for supporting this work. A. Sengupta thanks the Luxembourg National Research Fund's ATTRACT Investigator Grant (Grant no. A17/MS/11572821/MBRACE) and CORE Grant (C19/MS/13719464/TOPOFLUME/Sengupta) for supporting this work.

Author contributions

Conceived and Designed: A.P. and M.Y., Data collection and Compilation: A.P., Data Analysis, and Interpretation: A.P., A.S., and M.Y., with A. S., and M.Y. supporting in specific analyses, Conclusions: A.P, A.S., and M.Y., Initial Draft: A.P., Revision and Final editing: A.P., A.S., and M.Y., and Overall Supervision: A.P.

Declaration

Competing interests

The authors declare no competing interests.

Additional information

Supplementary Information The online version contains supplementary material available at https://doi.org/10.1038/s41598-024-73836-4.

Correspondence and requests for materials should be addressed to A.P.